A device for measuring tactile spatiotemporal sensitivity

Clayton L. Van Doren, Denis G. Pelli, and Ronald T. Verrillo
Institute for Sensory Research, Syracuse University, Syracuse, New York 13244-5290

(Received 12 September 1986; accepted for publication 7 March 1987)

A tactile stimulator array constructed from 88 piezoelectric ceramic plates is described. The array can produce sinusoidal traveling waves with arbitrary temporal frequency, spatial wavelength, and amplitude. Detection thresholds were measured for five temporal frequencies (1, 4, 16, 64, and 256 Hz) and five spatial wavelengths (1.81, 3.62, 7.23, 14.5, and ∞ mm), and were plotted as a three-dimensional, spatiotemporal threshold surface. Detection thresholds were also measured using a conventional vibrator and a large circular contactor simulating the infinite wavelength stimulus produced by the array. The results describe the spatial and temporal frequency sensitivity of the P and NP I cutaneous receptor populations.

PACS numbers: 43.66.Wv, 43.88.Fx, 43.40.Ng [DW]

INTRODUCTION

In the mid-1800s, Louis Braille developed a system for translating the written alphabet into a code of raised dots that can be "read" when touched by the fingertips. The use of this code by blind readers is an example of the ability of the skin to discriminate spatial patterns and provide information that would otherwise be acquired visually. Even in normal use, the skin is used to detect, resolve, and identify textures and shapes. It is important, therefore, to know how the skin acquires and uses spatial and temporal information in order to understand its normal function and to improve upon its use as an alternate channel for visual or auditory communication.

A significant step in understanding skin function is the development of a descriptive model for its responses. The model is complete when it can accurately predict the skin's response to an arbitrary stimulus. Usually, the prediction is based upon previously recorded responses to simpler stimuli. A complex stimulus is decomposed analytically into a finite number of these simple stimuli, each producing a known response. The component responses are then combined according to the rules of the model, yielding a predicted response to the complex stimulus.

For example, a visual pattern can be interpreted as a collection of features such as lines, edges, and shapes, or as a superposition of spatial sinusoids, i.e., Fourier components. Responses to both types of components have been recorded (e.g., Hubel and Wiesel, 1962; Enroth-Cugell and Robson, 1966) and can, with an appropriate model, be used to predict the response to a more complex pattern. It is not clear, *a priori*, that either features or sinusoids are particularly well suited for stimulating the visual system or approximating "natural" stimulation, but sinusoids have at least one major advantage—they are uniquely suited for the application of *linear* system analysis to the relationship between the stimulus and the response (e.g., Shapley and Lennie, 1985).

If a sinusoid is presented to the input of a linear system, then a sinusoid of the same frequency will appear at the output, although it may have a different amplitude and phase. In fact, a record of the output amplitude and phase as a function of input frequency completely characterizes a linear system and can be used to predict the system's response to an arbitrary input. Therefore, if the system is linear, this analysis immediately satisfies the principal requirement of a descriptive model. If the system is nonlinear, a sinusoidal input will typically produce a distorted sinusoid, with multiple frequencies, at the output. Even so, there may be limited ranges where the response is linear, or the distortions may be small enough to either permit a linear approximation or suggest minor modifications of the linear model. If the distortions are pronounced, they may identify the nature of the nonlinearity, such as a threshold, saturation, or rectification. In any case, the use of sinusoids provides useful information about the system.

It seems reasonable, then, to attempt a linear characterization of tactile response using sinusoidal stimuli and to make corrections to the model as demanded by any observed departures from linearity. In the past, many investigations have used a variety of stimulators to deliver spatiotemporal patterns to the skin, but none is well suited for linear analysis. Some, like the electromagnetic vibrator (Setzepfand, 1935; Sherrick, 1953; Verrillo, 1962), can produce an accurate temporal sinusoid, but the spatial pattern is a simple shape, such as a disk, rather than a sinusoid. Other stimulators, such as square gratings (Lederman and Taylor, 1972; Darian-Smith and Oke, 1980; Johnson and Phillips, 1981; Morley *et al.*, 1983) or sandpaper (Stevens and Harris, 1962; Lederman and Abbot, 1981; Heller, 1982), can vary the spatial and temporal frequency spectra, but cannot produce spatial or temporal sinusoids.

A more suitable stimulus for linear analysis is the drifting sinusoidal grating similar to that used in vision experiments (e.g., Robson, 1966), where the luminance of the pattern varies sinusoidally with position and time. This pattern can be described by the equation for a traveling wave,

$$y(x,t) = A \sin[2\pi(\nu x - f_0 t)], \quad (1)$$

where y is the stimulus amplitude as a function of position x and time t, A is the maximum amplitude, f_0 is the temporal frequency, and ν is the spatial frequency. The spatial frequency is equal to the inverse of the spatial wavelength λ. As a tactile stimulus, this pattern will be a sinusoidal wave propagating over a surface in contact with the skin. The goal of this project was to construct a device capable of producing such spatiotemporal sinusoids.

 0001-4966/87/061906-11$00.80

I. APPARATUS

A. Specification

The device should generate traveling waves over the expected range of temporal frequencies, spatial frequencies, and amplitudes to which the skin is sensitive. Since sensitivity changes with body location (Ruch, 1946; Weinstein, 1968), a single test site, the index fingertip, was chosen for the investigation. The fingertip was selected because it has a high spatial acuity (Ruch, 1946; Weinstein, 1968) and is the principal area used for tactile exploration. In a study of tactile spatial resolution, Johnson and Phillips (1981) measured two-point discrimination, gap detection, grating resolution, and letter recognition in order to estimate the limit of human tactile spatial acuity for stimuli applied to the fingertip. Their results suggest that spatial features smaller than about 0.5 mm cannot be resolved. Therefore, the device should be able to produce wavelengths as short as 0.5 mm. At the other extreme, the longest wavelength should be infinite, but the size of the stimulator only needs to be as large as the fingertip, which has dimensions on the order of 15×25 mm.

The desired temporal bandwidth can be inferred from earlier experiments that used simple vibrators. Human thresholds have been measured from 0.5–400 Hz physiologically (Johansson *et al.*, 1982a) and from 0.2 (Bolanowski, Jr., 1986) to 1000 Hz (von Békésy, 1939) psychophysically, suggesting an appropriate temporal bandwidth of 0–1000 Hz.

Finally, detection thresholds of known cutaneous receptor populations may range from 0.1- to 100-μm zero-to-peak displacement (Gescheider *et al.*, 1985).

These operating specifications for the device are summarized in Table I, along with the restrictions they place on the stimulator design. Independent control of temporal frequency and spatial wavelength implies that the device must be an array of independent vibrators. While traveling waves can be produced on the surface of a continuous, elastic material, such as rubber, the spatial wavelength, temporal frequency, and propagation velocity are interdependent. An array, on the other hand, can discretely approximate a surface wave of arbitrary spatial and temporal frequency by controlling the displacements of the individual elements, as shown in Fig. 1.

The required spatial bandwidth (or range of wavelengths), shown in Table I, determines the size of elements in the array. Shannon's sampling theorem requires that the waveform be represented by at least two elements per cycle, which demands that each element be no more than 0.25 mm thick. To cover the 25-mm length of the fingertip requires 100 such elements. Furthermore, each element of the array must have the temporal frequency response and dynamic range already specified for the device as a whole. Therefore, the critical component is the individual vibrating element, which must be, at most, 0.25 mm thick, and must have a dynamic range of at least 0.1–100 μm and a frequency response of at least 0–1000 Hz.

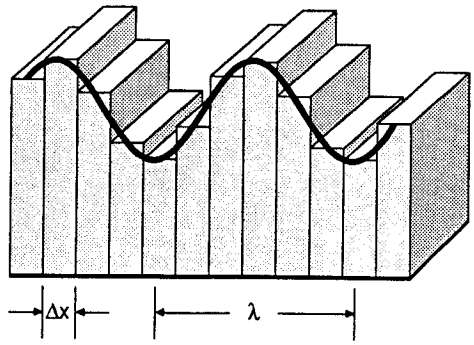

FIG. 1. Schematic drawing showing the upper surface of an array of vibrating elements used to discretely approximate a traveling wave. The displacement of each plate is determined from the equation $y_i(x_i,t) = A \sin\{2\pi[(x_i/\lambda) - ft]\}$, where y_i is the vertical displacement of the ith element at a position $x_i = i\,\Delta x$. Δx is the element thickness, λ is the spatial wavelength, and f is the temporal frequency.

B. Design

Nearly all of the requirements can be satisfied by using a thin, piezoelectric ceramic plate as the vibrating element. The array, as constructed, uses 124-$\times$25-$\times$0.25-mm plates of a lead zirconate–lead titanate ceramic (PZT-5J, available from Vernitron Piezoelectric Division, Cleveland, OH). The plates are thin enough for a minimum wavelength of 0.5 mm, but the frequency response and dynamic range depend in a complex way on the dimensions and material constants of the plate.

The basic dynamic behavior of a single plate is shown schematically in Fig. 2. The plate has rest dimensions of length L_1, width L_2, and thickness L_3, and an intrinsic polarization **P** produced during manufacture. By convention, the direction of the polarization defines the **3** axis of the material, and the **1** and **2** axes complete the orthogonal coordinates. As shown in Fig. 2(b), an electric field **E** applied

TABLE I. Summary of device specifications. Independent control of temporal frequency and spatial wavelength requires an array of independent vibrating elements. The stimulus requirements and the restrictions placed on the elements and the array are given in the table, along with the performance actually realized by the completed device.

Stimulus parameters	Stimulus specifications	Element specifications	Element performance	Array performance
Range of wavelengths	0.5–∞ mm	$\leq$0.25 mm thick	0.38 mm thick	0.76–∞ mm
Contact area	25×15 mm	$\geq$100 elements, $\geq$15 mm wide	88 elements, 19.0 mm wide	33.4×19.0 mm
Temporal bandwidth	0–1000 Hz	0–1000 Hz	0–1000 Hz	0–1000 Hz
Dynamic range	0.1–100 μm	0.1–100 μm	0.03–11 μm	0.03–11 μm

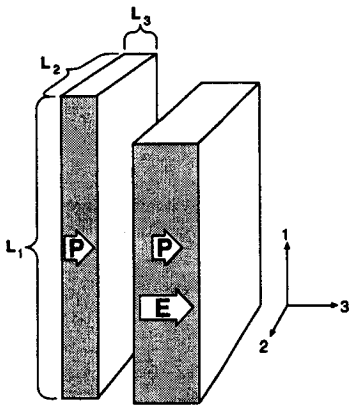

FIG. 2. The basic behavior of a piezoelectric ceramic plate. At rest, the plate has dimensions of length L_1, width L_2, and thickness L_3. There is an intrinsic polarization **P** that defines the direction of the **3** axis. The **1** and **2** axes complete the orthogonal coordinates. An electric field **E** applied across the plate in the direction of the original polarization produces elongation of L_3 and contraction of L_1 and L_2.

in the direction of the polarization will produce expansion along the **3** axis and concomitant contraction along the **1** and **2** axes. For electric fields well below the depolarization strength of the material, usually several thousand V/cm ("Piezoelectric Technology, Data for Designers," Vernitron Piezoelectric Division), and temporal frequencies well below the mechanical resonance of the plate, the relationship between the change in length along the **1** axis and the applied field can be described by the linear equation (Berlincourt, 1984)

$$S_1 = d_{31}E_3, \tag{2}$$

where S_1 is the strain in the **1** direction (i.e., the proportional change in length), E_3 is the applied field in the **3** direction, and d_{31} is a material constant. Since

$$S_1 = \Delta L_1/L_1, \tag{3}$$

where ΔL_1 is the absolute change in length, and

$$E_3 = V/L_3, \tag{4}$$

where V is the voltage applied across the plate, Eq. (2) can be reexpressed as

$$\Delta L_1 = (d_{31}L_1/L_3)V. \tag{5}$$

That is, the change in length is directly proportional to the applied voltage V, and the constant of proportionality depends solely on the material and its dimensions.

Although the temporal frequencies of interest are well below the plate's mechanical resonance frequency of roughly 10 kHz, estimated from a resonance frequency nomagraph (Modern Piezoelectric Ceramics, publication PD-9247, Vernitron Piezoelectric Division), the linear function of Eq. (2) is just an approximation to the actual strain–field relation. The actual strain–field function exhibits an accelerating nonlinearity and hysteresis (Berlincourt, 1984). As discussed by Berlincourt (1984), these nonlinearities restrict the maximum usable voltage in two ways. First, they cause waveform distortion that increases as the voltage increases. Second, the nonlinearities produce dielectric heating of the material, increasing with both voltage and frequency, which can result in depolarization and loss of the piezoelectric response. Therefore, the maximum voltage is determined by the acceptable amount of distortion and the heat tolerance of the material. Both effects are more pronounced at negative voltages, i.e., voltages applied opposite to the direction of the intrinsic polarization. Measurements of plate capacitance and displacement over the temporal bandwidth of interest indicate that stable operation with minimal distortion can be maintained using positive, unipolar sinusoids having a dc offset of 150 V and a maximum ac amplitude of 150 V.

As a first approximation, the linear relation in Eq. (5) predicts a 17-μm zero-to-peak displacement (i.e., sinusoidal amplitude) for a 124-mm-long plate of PZT-5J with a d_{31} constant of -230×10^{-12} m/V (sheet #9247-10, 1983, Vernitron Piezoelectric Division). This displacement could be increased by using a longer plate or a material with a larger d_{31} constant. Unfortunately, the 124-mm plate is the longest available, and the only material with a larger d_{31} constant (-270×10^{-12} m/V, PZT-5H, Vernitron Piezoelectric Division) was found to be less stable at the same maximum voltage. A maximum amplitude of 17 μm is much less than the 100 μm specified in Table I, but should be sufficient to produce tangible stimuli for many combinations of spatial and temporal frequencies.

After selection and testing, the plates were assembled into an array, as shown in Fig. 3. To provide electrical and mechanical isolation of adjacent plates, each plate was painted with Dow Corning 997 varnish (Dow Corning Corporation, Midland, MI) and lubricated with a dry teflon aerosol (#708, Sprayon Industries, Bedford Heights, OH). As a consequence of coating the plates with varnish and teflon, the total average thickness of the plates increased from 0.25 mm to 0.38 mm, increasing the minimum usable wavelength from 0.50 mm to 0.76 mm. The final array contained 88 plates for a total length of 33.4 mm. As indicated in Fig. 3, the plates were staggered in order to accommodate lead wires. As a result, the useful width of the array was 19 mm. The array and its enclosure were subsequently assembled into a unit that mounted directly onto a vibration-isolated table.

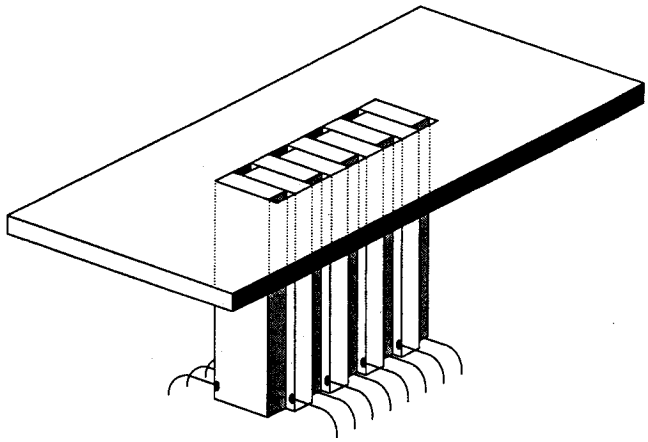

FIG. 3. Simplified drawing of the assembled array, not drawn to scale, with only 9 of the 88 plates shown. The plates are staggered to accommodate wires soldered near the bottom on either side of each plate. The enclosure for the array is not shown.

The array of plates, however, is only one part of the whole apparatus. The complete system used to produce the stimulus is shown in the block diagram of Fig. 4. The microcomputer, an LSI-11/73 (Digital Equipment Corp., Maynard, MA), calculates the data necessary to digitally synthesize the stimulus, stores the data in memory, and sends the data to the peripheral hardware via a direct-memory-access card (DMA-Q, modified to have a maximum transfer rate of 1 Mbyte/s and unlimited length of data transfer, Peritek Corp., Oakland, CA). The data leave the computer as a single stream of 88 serially multiplexed signals. This data stream is subsequently divided into 88 parallel data paths by a custom-built demultiplexor that also controls the signal timing and the rate of data transfer. Each of the 88, 8-bit data streams is converted into an analog signal by a digital-to-analog converter, amplified by one of 88 plate drivers, and applied across a plate in the array.

Since the plates act as capacitive loads, they draw more current at higher frequencies. The typical capacitance of a single plate is 250 μF, which at 1000 Hz yields an impedance of 159 Ω. Therefore, each of the 88 plate drivers must be able to supply a current of 167-mA rms at 150 V zero to peak (106-V rms). A schematic of the plate driver is shown in Fig. 5. Alternatives to the bipolar transistors were considered, such as high-power op-amps and power MOSFETs, but were discarded because components available at the time could not deliver the necessary current at the desired voltage. The drivers, as constructed, operate with a high-voltage supply of 325 V, draw a maximum current of 185-mA rms at 1000 Hz and 150-V zero-to-peak output, and have a gain of 50 over a bandwidth of 0–1000 Hz.

The input voltage to the plate drivers is supplied by 8-bit, multiplying, digital-to-analog converters (MDACs). The output v_i of each MDAC is the product of two input signals, an 8-bit digital number n_i, where i is the channel number, and a reference voltage, v_{ref}, common to all 88

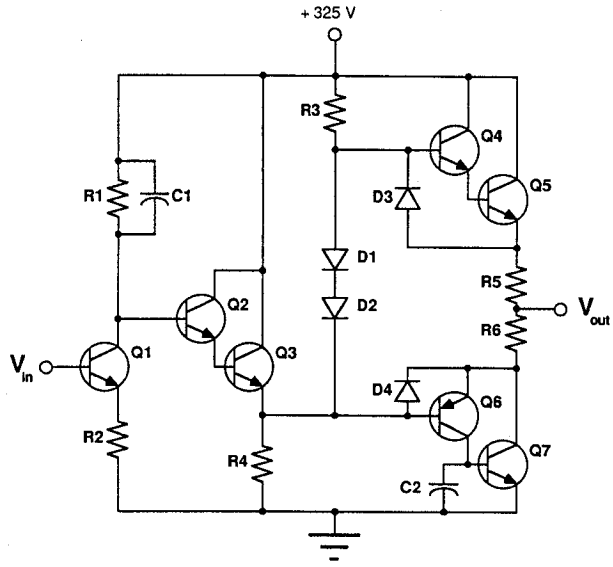

FIG. 5. Schematic circuit diagram of the plate drivers. Here, R 1, R 2, and Q 1 form a common-emitter amplifier and provide a voltage gain of 50; Q 2 and Q 3 operate as a Darlington pair and provide the current amplification to drive the output stage. The output stage consists of the Darlington pairs Q 4–Q 5 and Q 6–Q 7 operating in a push–pull mode. For a more detailed discussion of this circuit, see Horowitz and Hill (1980).

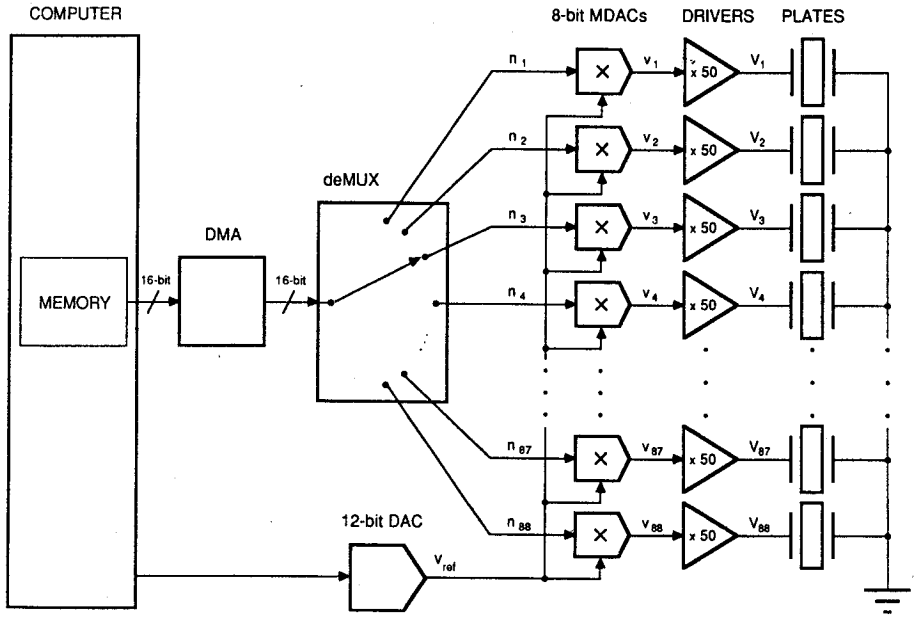

FIG. 4. Block diagram of the apparatus. The computer calculates and stores the stimulus data in memory. The direct-memory-access card (DMA) reads the data from memory and outputs them as a single stream of 88 serially multiplexed signals. The data stream is demultiplexed (deMUX) into 88 parallel 8-bit streams. The 8-bit numbers n_i are converted to low-voltage analog signals v_i by separate multiplying digital-to-analog converters (MDACs). The outputs of the MDACs are the product of n_i and a common, computer-controlled reference voltage v_{ref} supplied by a 12-bit DAC. The low-voltage signals v_i are then amplified by the plate drivers, producing the high-voltage signals V_i that are applied across the plates in the array.

channels:

$$v_i = (n_i/255)v_{\text{ref}}. \quad (6)$$

The reference voltage, used to control the overall amplitude of the signal, is computer controlled and supplied by a single 12-bit digital-to-analog converter. Theoretically, the 12-bit resolution of v_{ref} should afford a 72-dB dynamic range, but capacitive feedthrough in the multiplier sections of the 8-bit MDACs reduced the usable range to 50 dB.

Finally, the demultiplexor (deMUX) establishes an overall data transfer rate of 8192 bytes/s per channel, which is more than enough for synthesis of the maximum stimulus frequency of 1000 Hz. At this transfer rate, the available computer memory (about 1 Mbyte) limits the total duration of a precalculated stimulus to 1.25 s.

A similar device has been constructed by Park *et al.* (1985) to produce traveling waves designed to cancel Tollmien–Schlichting waves in a laminar boundary of moving fluid. Their 32-element array uses piezoelectric ceramic plates (spaced on 1.25-mm centers), has a frequency bandwidth of 10–150 Hz, and has a maximum sinusoidal amplitude of 13 μm. Their traveling wave is produced by a signal generator and a digital shift register followed by 8-bit DACs and VMOSFET plate drivers.

C. Calibration

The displacements of individual plates in the array were measured using a ceramic phonograph cartridge mounted on a base permitting micrometer-driven height adjustment. The cartridge and its amplifier were calibrated using an electromagnetic vibrator and an optical displacement transducer (Fotonic Sensor KD-100, MTI Instruments Division, Latham, NY).

After a preliminary examination, it became apparent that the array's response was distorted and nonlinear, so detailed measurements were made in order to characterize the behavior of the array. The deviations from linearity arise from two sources: the nonlinearity and hysteresis of the strain–field relationship for an isolated plate (Berlincourt, 1984), mentioned in the discussion of Eq. (5), and the mechanical coupling between adjacent plates in the array. It will be shown that the latter is more important.

Empirically, the most serious nonlinearity is the relation between amplitude and driving voltage. As shown in Fig. 6,

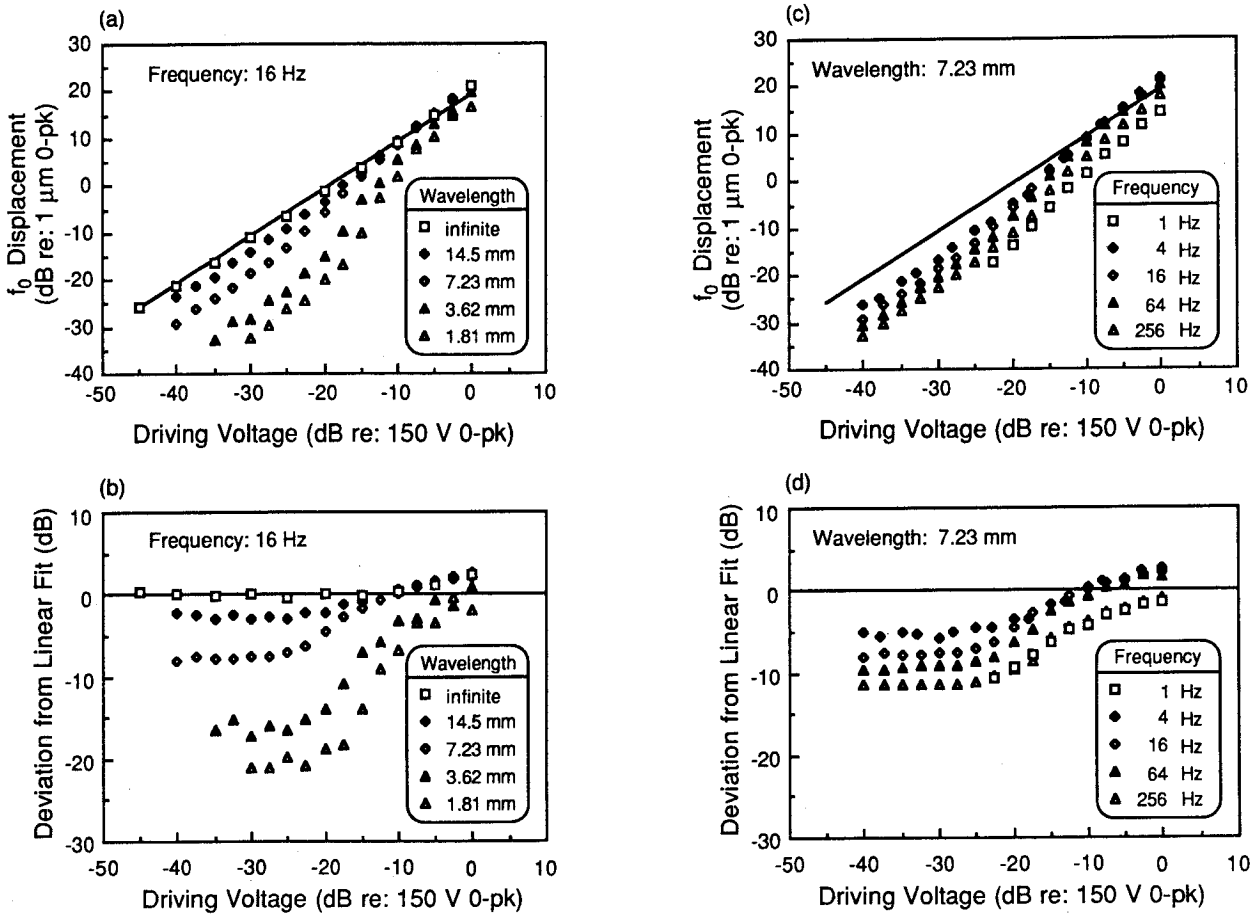

FIG. 6. Amplitude of the plate displacement at the fundamental frequency f_0 as a function of the amplitude of the sinusoidal driving voltage for several spatial wavelengths and temporal frequencies. The f_0 displacement was measured from a Fourier transform of the calibrating phonograph cartridge voltage. (a) The f_0 displacement (in dB *re*: 1 μm zero to peak) plotted as a function of driving voltage (in dB *re*: 150 V zero to peak) at a temporal frequency of 16 Hz and 5 wavelengths: 1.81, 3.62, 7.23, 14.5, and ∞ mm. The straight line, a least-squares fit to the infinite-wavelength data for voltages of -10 dB and below, has a slope of 1.00 and a regression coefficient of 1.00. A slope of 1 represents linearity (i.e., displacement proportional to driving voltage). (b) The displacements (in dB) predicted by the linear fit in (a) are subtracted from the measured displacements (in dB), and the differences are plotted as a function of driving voltage. Note that, even for an infinite wavelength, there is a departure from linearity at the highest driving voltages. (c) The f_0 displacements are plotted as in (a), but at a constant wavelength of 7.23 mm and five temporal frequencies: 1, 4, 16, 64, and 256 Hz. The line is the same as in (a). (d) As in (b), the deviations from the linear fit of (a) are plotted as a function of driving voltage.

the displacement of a plate in the array depends not only on the driving voltage, but also on the temporal frequency and spatial wavelength of the stimulus. Figure 6(a) shows a family of curves plotting the amplitude of the displacement at the fundamental stimulus frequency (referred to hereafter as the f_0 displacement) as a function of the driving voltage for a constant temporal frequency and several spatial wavelengths. The f_0 displacement was determined by taking a Fourier transform of the phonograph cartridge voltage and measuring the amplitude of the fundamental component. The nonlinearity is worse for short wavelengths where the relative motion of adjacent plates is greatest, implying that the deviations are primarily due to mechanical coupling between the plates. However, at an infinite wavelength, all the plates move with the same phase and there is no relative motion between plates. Even so, there is a small deviation from linearity at high voltages as seen in Fig. 6(a) and more clearly in Fig. 6(b), where the deviation from linearity is plotted directly as a function of the input voltage. Therefore, the residual nonlinearity at an infinite wavelength must be due to departures from the linear relation between the applied voltage and the displacement isolated plate shown in Eq. (5), and not due to mechanical coupling between plates in the array.

It might also be expected that a nonlinearity due to the relative motion of the plates would increase with temporal frequency. Figure 6(c) shows another family of amplitude-voltage curves at a constant wavelength and several temporal frequencies. As expected, the nonlinearity tends to increase as frequency increases, but the effect is much more subtle than the changes due to wavelength. Oddly, the trend is nonmonotonic since the nonlinearity decreases from 256 to 4 Hz, but increases again at 1 Hz.

Although a detailed physical explanation for the nonlinearities is not currently available, it is possible to correct for *some* of the distortions they produce by changing the analog attenuation in order to linearize the f_0 displacement. The waveform will still be distorted, however, because the correction ignores harmonic distortion.

In order to implement this correction it was necessary to measure the f_0 displacement as a function of input voltage for all combinations of frequency and wavelength used in the experiment. Some of these functions are shown in Fig. 6(a) and (c). A cubic equation was fit to the data by the method of least squares. This function, describing the f_0 displacement (in dB) produced by a given input voltage (in dB), was inverted to produce a function that returns the input voltage necessary to attain a particular f_0 displacement. The inverted function was then used in the computer program controlling the stimulus attenuation to compensate for the effect of the nonlinearity. An example of the correction is shown in Fig. 7 for one of the worst cases. Figure 7(a) shows the f_0 displacement versus voltage for a frequency of 4 Hz and a wavelength of 1.52 mm. The continuous curve drawn through the data is a least-squares cubic fit with a regression coefficient of 0.998. Figure 7(b), on the other hand, shows a plot of the measured f_0 displacement versus the programmed f_0 displacement. The difference between the measured displacement and the programmed displacement is 2 dB or less.

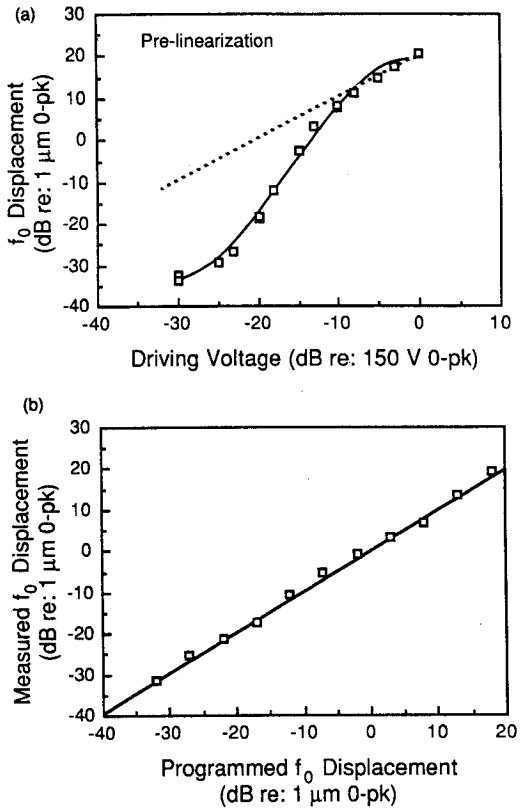

FIG. 7. (a) Plot of f_0 displacement (in dB) at the fundamental frequency as a function of driving voltage (in dB) for a frequency of 4 Hz and a wavelength of 1.52 mm. The solid line is a least-squares cubic fit to the data. The dashed line represents linearity. (b) Measured f_0 displacements plotted versus programmed f_0 displacements following the linearization procedure. The line has a slope of 1.00 and represents equality between measured and programmed displacements. The maximum disparity between measured and programmed displacements is 1.8 dB.

As mentioned earlier, linearization of the f_0 displacement does not compensate for harmonic distortion of the waveform. The amount of distortion produced by the nonlinearities was measured by taking the Fourier transform of the calibrating phonograph cartridge voltage, and measuring the peaks in the spectrum at the harmonic frequencies. The most prominent distortion component was the third harmonic. As shown in Fig. 8, the total harmonic distortion (THD, the rms sum of the harmonic amplitudes divided by the amplitude of the fundamental $\times 100\%$) decreases with spatial wavelength and increases with temporal frequency, with a maximum THD of 12%. The minimum THD, less than 2%, occurs at an infinite wavelength, again suggesting that the intrinsic strain–field nonlinearity and the hysteresis of the material are small compared to the nonlinearities due to mechanical coupling.

In addition to stimulus nonlinearities, there are also two sources of spatial inhomogeneity. Nominally, the plates are evenly spaced on 0.38-mm centers. After the array was assembled, however, electrical shorts developed between several pairs of adjacent plates. Since the plates could not be removed from the array, 100-μm plastic shims were placed between the affected plates. Therefore, at these locations, there are local variations in the nominal wavelength. Although it is difficult to predict how the shims will affect

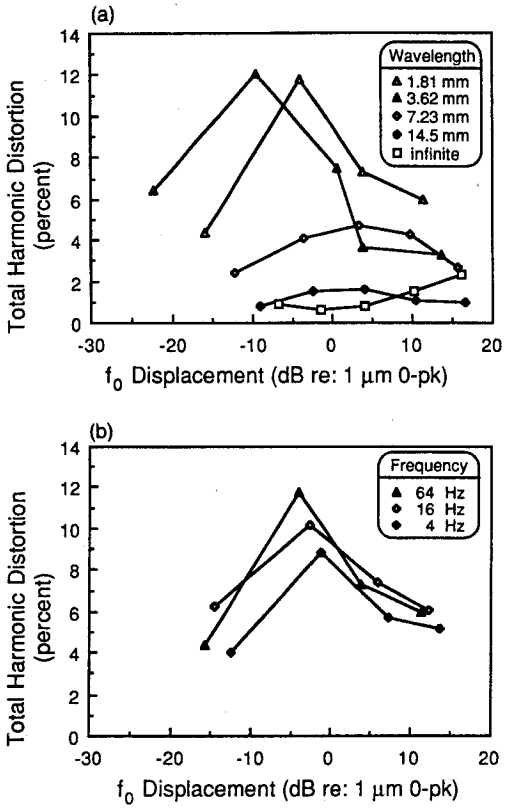

FIG. 8. Total harmonic distortion (THD) plotted as a function of f_0 displacement. (a) THD for a constant temporal frequency of 64 Hz and 5 wavelengths: 1.81, 3.62, 7.23, 14.5, and ∞ mm. (b) THD for a constant wavelength of 1.81 mm and three frequencies: 4, 16, and 64 Hz.

detection thresholds, their effect is expected to be small since they only produce a 20% increase in the center-to-center spacing of adjacent plates, with a proportionally smaller perturbation of wavelengths that span several plates.

The second source of spatial inhomogeneity arises from the differences in the displacement of different plates at the same voltage. This variation is due to differences in the d_{31} constant from plate to plate and to the local mechanical coupling at different sites in the array. To quantify the variation, peak displacements (not f_0 displacements) were measured from seven nonadjacent plates near the center of the array

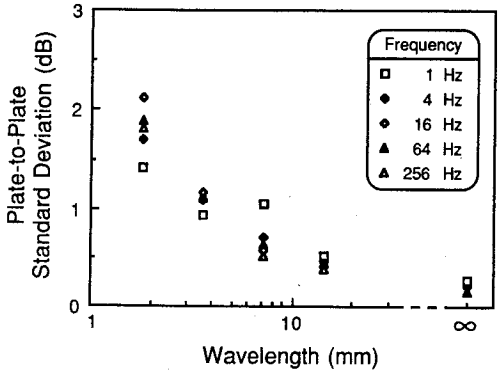

FIG. 9. Standard deviations of peak displacement measurements from seven nonadjacent plates in the array. The displacement at each frequency and wavelength combination was the maximum available, approximately 21 dB *re*: 1 μm zero to peak.

for all combinations of spatial wavelength and temporal frequency used in the experiment below. The standard deviations of the measurements, shown in Fig. 9, are, at most, 2.2 dB and decrease as spatial wavelength increases. In fact, the standard deviation approaches zero at an infinite wavelength, indicating that the differences in the d_{31} constant from plate to plate are much smaller than the differences in the local mechanical coupling.

To summarize, linearization of f_0 displacement worked reasonably well, although there is still a residual uncertainty of at most 2 dB for any amplitude at a given spatial wavelength and temporal frequency. The standard deviation of the average displacement across the array, as approximated by the samples of seven plates, is generally 2 dB or less. Therefore, the uncertainty in stimulus amplitude at any point is at most 4 dB.

D. Discussion

As a whole, the device nearly satisfies the original specifications in Table I. The thickness of the plates permits synthesis of wavelengths as short as 0.76 mm, over the 33.4-mm length of the array. The bandwidth and current-handling capability of the plate drivers allow a frequency range of 0–1000 Hz, and the available computer memory sets a maximum duration of 1250 ms. In short, the array successfully produces traveling sinusoids over the spatial and temporal frequency ranges of interest.

However, the array has one fundamental limitation: a maximum displacement of about 11 μm zero to peak. This is an unavoidable limitation of the plates themselves, and there is no obvious way to improve the performance using existing piezoelectric ceramic technology.

The array also suffers from nonlinearities and distortions produced by the mechanical coupling between the plates. In hindsight, it is clear that the lubrication of the plates was unsuccessful, and a different strategy for isolating the plates is called for. The array is being redesigned to eliminate the plate-to-plate coupling.

In the current device, the principal consequence of the coupling is to require extensive calibration measurements to allow linearization of the displacement at the fundamental frequency. Following the linearization, however, harmonic distortion and spatial inhomogeneities remain. The effects of these distortions are expected to be small, and no attempt was made to correct for them.

II. PILOT EXPERIMENT

Tactile detection thresholds for sinusoidal traveling waves were measured as a function of spatial wavelength and temporal frequency. This experiment is analogous to the vision study of Robson (1966).

A. Method

The experiment measured detection thresholds at the left index fingertip (ventral surface of the distal phalanx) for stimuli presented by the stimulator array at all combinations of five wavelengths (1.81, 3.63, 7.23, 24.5, and ∞ mm) and five frequencies (1, 4, 16, 64, and 256 Hz). In addition, detection thresholds were measured at ten frequencies (1, 2, 4,

8, 16, 32, 64, 128, 256, and 512 Hz) using a flat, circular contactor, 25.7 mm in diameter, attached to a conventional electromagnetic vibrator. The single, large contactor was equivalent to the infinite wavelength stimulus produced by the array, and could produce much larger displacements than the array (up to several mm). The single contactor was used to measure infinite-wavelength thresholds inaccessible to the array and to provide a direct comparison between the performance of the array and that of a conventional stimulator.

To accommodate the 1-Hz stimulus and to minimize the effects of temporal summation (Verrillo, 1965), all stimuli had a temporal envelope with a half-power[1] duration of 600 ms and a rise–fall time of 500 ms using sine-squared skirts. The total duration was 1236 ms.

No spatial envelope was used because the contact area of the fingertip was smaller than the active area of the array. Since the fingertip did not overlay any edge of the array, the array was effectively of infinite extent. The vignetting of the stimulus resulted from the curvature at the edge of the fingertip, which gradually lifts the skin away from the surface of the array. The same analysis holds for the single contactor.

For stimuli presented with the array, the subjects' thresholds were determined using a two-alternative, forced-choice tracking paradigm called *QUEST* (Watson and Pelli, 1983). For each run, the subject responded to 40 stimulus presentations and *QUEST* calculated a maximum likelihood estimate of threshold for the set of responses. Threshold was defined as a 92% correct-response rate, which minimizes the ideal sweat factor (Taylor, 1971; Watson and Pelli, 1983). If this criterion occurred at a stimulus amplitude above the maximum amplitude that could be produced by the array, *QUEST* extrapolated to the threshold along a template of the psychometric function. However, extrapolations greater than 3 dB implied that the subject was operating at a correct-response rate below 70%, and were rejected.

For stimuli presented by the contactor and vibrator, thresholds were measured using the two-alternative, forced-choice tracking paradigm of Zwislocki *et al.* (1958). This method has been used in many previous studies with conventional stimuli (e.g., Gescheider *et al.*, 1983, 1985; Bolanowski *et al.*, 1982). The tracking rule used in this method (every third correct response decreases the stimulus amplitude by 1 dB, and every incorrect response increases the amplitude by 1 dB) converges to a 75% correct-response rate. Therefore, thresholds measured using this rule should be slightly lower than those measured by *QUEST*. However, the expected difference (about 2.5 dB) is smaller than the standard deviation of the data.

For thresholds measured with the array, an experimental session consisted of five runs, one for each spatial wavelength, presented in random order. All five runs in a session were at the same temporal frequency (1, 4, 16, 64, or 256 Hz). Each session lasted 30 min, including 2-min rest periods between runs. The subjects were also given a 10-min rest between sessions. For the single contactor measurements, each session consisted of five runs at frequencies randomly chosen from the set of ten (1, 2, 4, 8, 16, 32, 64, 128, 256, or 512 Hz). Again, sessions lasted for 30 min and subjects were given 10-min rest between sesssions. Throughout a session for either stimulus, the subjects sat in a sound- and vibration-isolated booth, and wore headphones presenting bandpassed noise to mask the sounds produced by the array or the vibrator.

B. Results and discussion

The results of this experiment are shown in Figs. 10–12. In Fig. 10, the detection thresholds are plotted as a function of both spatial wavelength and temporal frequency, producing a threshold surface in three dimensions. Each closed point is the grand mean of four threshold estimates from two subjects and three estimates from a third subject. The thresholds at an infinite wavelength are from the array (closed points) and the single contactor (open points, grand mean of four threshold estimates from three subjects). Although it is difficult to read the actual values of the thresholds from the surface, it is clear that thresholds generally decrease as frequency increases and as wavelength decreases.

To establish quantitative relations among the thresholds, it is convenient to construct a pair of two-dimensional projections of the three-dimensional surface. In Fig. 11, the surface has been projected onto the threshold versus temporal frequency plane. The projected curves, each showing the relation between threshold and temporal frequency at a single spatial wavelength, are analogous to frequency-tuning curves measured in earlier psychophysical (e.g., Verrillo, 1962; Gescheider *et al.*, 1985) and physiological (e.g., Talbot *et al.*, 1968; Johansson *et al.*, 1982a) studies.

Gescheider *et al.* (1985) used an electromagnetic vibrator and a 0.01-cm^2 circular contactor to demonstrate the existence of three receptor populations, designated NP I, NP II, and P, in glabrous skin. Of these, the P and NP I receptors mediate detection in the frequency range of 10–700 Hz, and are equivalent to the P and NP systems proposed in the du-

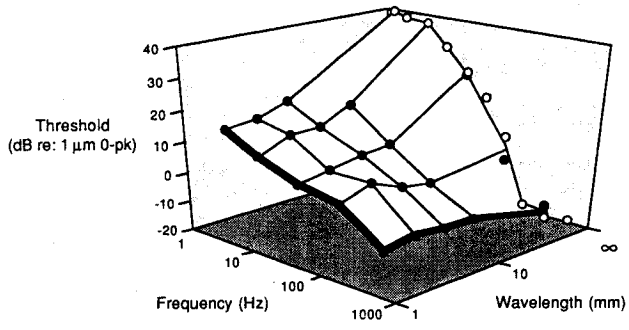

FIG. 10. Detection thresholds plotted simultaneously as a function of spatial wavelength and temporal frequency. Each closed point is the grand mean of four threshold estimates from two subjects and three threshold estimates from a third subject, measured using the tactile stimulator array. Open points are thresholds measured using a single contactor, 25.7 mm in diameter, and are the grand means of four threshold estimates from three subjects. Standard errors range from 0.5–3.7 dB, with a median value of 1.3 dB (error bars are shown in Fig. 12).

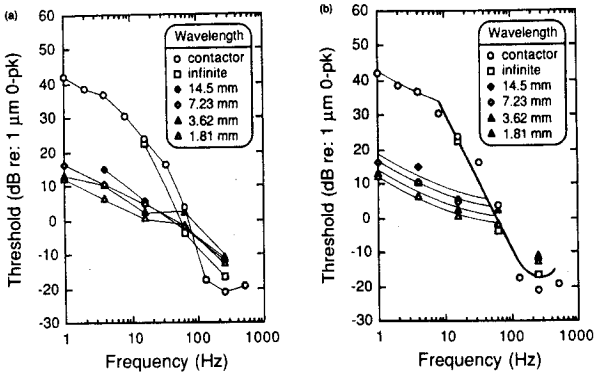

FIG. 11. (a) Detection thresholds as in Fig. 10 plotted as a function of temporal frequency with spatial wavelength varied parametrically (error bars are shown in Fig. 12). (b) The data in (a) are replotted with model threshold curves fit to the data by eye. The NP I threshold curves (thin lines) are replicas of the curve fitted to the 1.81-mm data and shifted vertically. The P threshold curve (thick line) is based on tuning characteristics from earlier studies. See text for discussion.

plex model of Verrillo (1966). Based on similarities to physiological tuning curves in monkey (Talbot *et al.*, 1968; Mountcastle *et al.*, 1972), cat (Sato, 1961; Bolanowski and Verrillo, 1982), and humans (Johansson *et al.*, 1982a), it is widely accepted that P thresholds are mediated by Pacinian corpuscles, and NP I thresholds are mediated by the physiologically classified RA receptors associated with Meissner's corpuscles (Lindblom, 1965).

Previous studies (Verrillo, 1962, 1966; Gescheider, 1976; Gescheider *et al.*, 1983) have clearly established a dichotomy between high-frequency detection by the P system and low-frequency detection by the NP I system. A similar interpretation is suggested in Fig. 11(a), where the slope is generally steeper above 64 Hz than below 64 Hz, indicating a transition from P detection to NP I detection. The transition between the two regions is at best suggestive because there

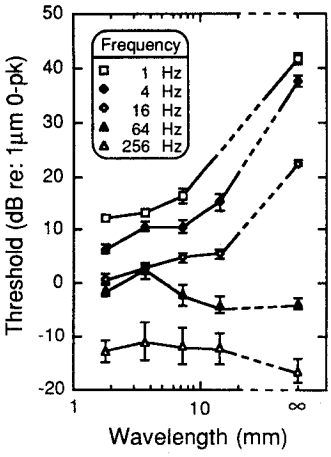

FIG. 12. Detection thresholds as in Fig. 10 plotted as a function of spatial wavelength with temporal frequency varied parametrically. Vertical bars show the standard error.

are too little data to clearly define the breakpoint for each spatial wavelength. However, the tentative model shown in Fig. 11(b) is at least consistent with both the data and the duplex theory of Verrillo (1966). The model is based on the *ad hoc* assumption that temporal tuning of a given receptor system is independent of spatial wavelength. Furthermore, the thresholds for a wavelength of 1.81 mm at frequencies from 1–64 Hz are presumed to be those of the NP I system. Under the assumption of tuning independence, the curve connecting these points is shifted vertically to fit the thresholds for the other wavelengths at low frequencies. In general, the low-frequency thresholds at any wavelength are adequately fit by this single NP I frequency characteristic, which is consistent with the original assumptions. At high frequencies, the data are fit with a typical P system threshold curve (Verrillo, 1966; Bolanowski and Verrillo, 1982) with the characteristic -12 dB/oct slope at low frequencies and a best frequency between 200 and 300 Hz.

In addition to accounting for the dependence of threshold on temporal frequency, the model also suggests that NP I thresholds increase as spatial wavelength increases and that P thresholds are only slightly affected by changing wavelength. Although the changes in the NP I thresholds at the three lowest frequencies and four shortest wavelengths are small, a two-factor analysis of variance shows that the variations with frequency and wavelength are both significant ($p < 0.005$). On the other hand, a similar analysis of the P thresholds at 64 and 256 Hz for all wavelengths indicates that the frequency variation is significant ($p < 0.005$), whereas the wavelength variation is not significant. This wavelength dependence of NP I thresholds and wavelength independence of the P thresholds are clearly demonstrated by projecting the threshold surface onto the threshold versus spatial wavelength plane, as shown in Fig. 12. These curves, showing the relation between threshold and spatial wavelength at different temporal frequencies, are analogous to contrast sensitivity functions measured for visual sinusoids (e.g., Robson, 1966) but are the first spatial tuning curves in tactile psychophysics. However, as suggested by the threshold characteristics fit in Fig. 11(b), the responses can still be interpreted according to the duplex model.

The threshold data in Fig. 12 show the *spatial* tuning characteristics of the P and NP I systems. The presumed NP I thresholds, measured at the three lowest temporal frequencies, decrease as the spatial wavelength decreases, indicating that the NP I system should respond preferentially to spatial gradients such as edges or points. Verrillo (1979) reached a similar conclusion by changing the gap between a small circular contactor and its surround. The threshold of the NP I system, measured at 25 Hz, increased as the gap increased, suggesting that the NP I system is sensitive to the spatial gradient produced between the edges of the contactor and the surround. Physiologically, both the RA and SA I receptors respond preferentially to edges (short spatial wavelengths) in monkeys (Phillips and Johnson, 1981), cats (Vierck, 1979), and humans (Johansson *et al.*, 1982b), but the SA I edge preference is more pronounced (Phillips and Johnson, 1981; Johansson *et al.*, 1982b). However, until a spatial tuning curve for a second NP system is measured, the

physiological identity of the NP I system cannot be confirmed.

Unlike the response of the NP I system, the P thresholds, measured at 64 and 256 Hz, are largely unaffected by changes in spatial wavelength. On the other hand, Verrillo (1963) measured the P threshold as a function of the size of a circular contactor and found that for diameters from 1.6 to 25.4 mm, the P threshold decreased 3 dB per doubling of contactor area, i.e., 6 dB per doubling of diameter. If the P system acts as a linear, low-pass spatial filter, as suggested by Verrillo's spatial summation results, then P thresholds should also decrease as spatial wavelength increases. Since the P thresholds in Fig. 12 decline only slightly with increasing wavelength, it is possible that spatial summation is instead a nonlinear process. The preliminary data shown here are insufficient, however, to suggest a particular mechanism for spatial summation.

III. CONCLUSIONS

An array of 88 piezoelectric, vibrating elements was constructed to explore tactile thresholds for sinusoidal traveling waves in three stimulus dimensions: temporal frequency, spatial wavelength, and amplitude. The array's performance nearly satisfies the original specifications—it can produce sinusoids with temporal frequencies from 0–1000 Hz and spatial wavelengths from 0.76–∞ mm, but has a range of displacements from 0.03–11 μm zero to peak, whereas tactile thresholds may range from 0.1–100 μm zero to peak. The device also has some distortion, primarily due to mechanical coupling between the plates. However, the array can still produce tangible sinusoidal traveling waves over a range of temporal frequencies and spatial wavelengths that is sufficient to distinguish the threshold responses of the NP I and P receptor populations. When plotted as a function of temporal frequency and spatial wavelength, the thresholds form a three-dimensional surface that describes tactile spatiotemporal sensitivity.

When the surface is projected onto the threshold versus *temporal* frequency plane, the resulting functions are analogous to frequency-tuning curves measured in previous investigations (Setzepfand, 1935; Talbot *et al.*, 1968) and agree with the duplex model of Verrillo (1966). The data are not intended to test the validity of the duplex model—this has been done in many previous experiments (e.g., Gescheider, 1976; Gescheider *et al.*, 1983; Verrillo, 1968)—but are consistent with these earlier results, and show, in part, the dichotomy between P and NP I responses.

On the other hand, the measurements of tactile thresholds as a function of *spatial* wavelength are the first of their kind. As in the temporal domain, the NP I and P systems can be differentiated by their threshold characteristics, but the differences are more apparent in the spatial domain. The NP I system responds best to short wavelengths (high spatial frequencies), whereas the P system is equally sensitive at all wavelengths. Again, these results agree with earlier physiological and psychophysical models.

In addition to discriminating between the P and NP I systems, the spatial-tuning curves provide the basis for predicting thresholds for more complex tactile gratings. Campbell and Robson (1968) and Campbell *et al.* (1969) used linear superposition to predict visual thresholds for square, rectangular, and sawtooth gratings, for half-cycle and single-cycle sinusoidal bars, and for the boundary between a sinusoidal grating and an unmodulated surround. For all stimuli, linear predictions agreed with empirical results within experimental error, except at low spatial frequencies (i.e., below 10 cycles/deg). A similar analysis can be applied to tactile thresholds to test for linearity of threshold response or confirm possible nonlinear responses such as spatial summation by the P system. All of the patterns used in the vision studies can be produced by the tactile array, and will provide the material for future investigation of spatiotemporal pattern perception.

ACKNOWLEDGMENTS

This research was supported by funds from the Allyn Foundation, Inc., Skaneateles, NY, by grants NS 09940, BRSG-S07RR077068-20, and EY 04432 from the National Institutes of Health, U.S. Department of Health and Human Services, and by a Syracuse University Graduate Fellowship. The authors would like to thank Evan M. Relkin for the use of the FFT equipment, and Arthur J. Wixson, Michael S. Schechter, Michael W. Serafini, and Robert W. Owen for their technical assistance.

[1]Half-power is defined as that time on the rising or falling edge of the envelope where the square of the envelope amplitude is equal to one-half of the square of the peak amplitude.

Békésy, G. von. (**1939**). "Uber die Vibrationsempfindung," Akust. Zh. **4**, 316–334.

Berlincourt, D. (**1984**). "Piezoelectric displacement generators—static and low frequencies," Tech. Pub. Channel Industries, Inc., Santa Barbara, CA.

Bolanowski, S. J., Jr., and Verrillo, R. T. (**1982**). "Temperature and criterion effects in a somatosensory subsystem: A neurophysiological and psychophysical study," J. Neurophysiol. **48**, 836–855.

Bolanowski, S. J., Jr. (**1986**). Personal communication.

Campbell, F. W., and Robson, J. G. (**1968**). "Application of Fourier analysis to the visibility of gratings," J. Physiol. **197**, 551–566.

Campbell, F. W., Carpenter, R. H. S., and Levinson, J. Z. (**1969**). "Visibility of aperiodic patterns compared with that of sinusoidal gratings," J. Physiol. **204**, 283–298.

Darian-Smith, I., and Oke, L. (**1980**). "Peripheral neural representation of the spatial frequency of a grating moving across the monkey's finger pad," J. Physiol. **309**, 117–133.

Enroth-Cugell, C., and Robson, J. G. (**1966**). "The contrast sensitivity of retinal ganglion celis of the cat," J. Physiol. **187**, 517–552.

Gescheider, G. A. (**1976**). "Evidence in support of the duplex theory of mechanoreception," Sens. Process. **1**, 68–76.

Gescheider, G. A., O'Malley, M. J., and Verrillo, R. T. (**1983**). "Vibrotactile forward masking: Evidence for channel independence," J. Acoust. Soc. Am. **74**, 474–485.

Gescheider, G. A., Sklar, B. F., Van Doren, C. L., and Verrillo, R. T. (**1985**). "Vibrotactile forward masking: Psychophysical evidence for a triplex theory of cutaneous mechanoreception," J. Acoust. Soc. Am. **78**, 534–543.

Heller, M. A. (**1982**). "Visual and tactual texture perception: Intersensory cooperation," Percept. Psychophys. **31**, 339–344.

Horowitz, P., and Hill, W. (**1980**). *The Art of Electronics* (Cambridge U. P., Cambridge, England), pp. 74–78.

Hubel, D. H., and Wiesel, T. N. (**1962**). "Receptive fields, binocular interaction, and functional architecture in the cat's visual cortex," J. Physiol. **160**, 106–154.

Johansson, R. S., Landstrom, U., and Lundstrom, R. (**1982a**). "Responses of mechanoreceptive afferent units in the glabrous skin of the human

hand to sinusoidal skin displacements," Brain Res. **244**, 17–25.
Johansson, R. S., Landstrom, U., and Lundstrom, R. (**1982b**). "Sensitivity to edges of mechanoreceptive afferent units innervating the glabrous skin of the human hand," Brain Res. **244**, 27–32.
Johnson, K. O., and Phillips, J. R. (**1981**). "Tactile spatial resolution. I. Two-point discrimination, gap detection, grating resolution, and letter recognition," J. Neurophysiol. **46**, 1177–1191.
Lederman, S. J., and Abbott, S. G. (**1981**). "Texture perception: Studies of intersensory organization using a discrepancy paradigm, and visual versus tactual psychophysics," J. Exp. Psychol.: Hum. Percept. Perform. **7**, 902–915.
Lederman, S. J., and Taylor, M. M. (**1972**). "Fingertip force, surface geometry, and the perception of roughness by active touch," Percept. Psychophys. **12**, 401–408.
Lindblom, U. (**1965**). "Properties of touch receptors in distal glabrous skin of the monkey," J. Neurophysiol. **28**, 966–985.
Morley, J. W., Goodwin, A. W., and Darian-Smith, I. (**1983**). "Tactile discrimination of gratings," Exp. Brain Res. **49**, 291–299.
Mountcastle, V. B., LaMotte, R. H., and Carli, G. (**1972**). "Detection thresholds for stimuli in humans and monkeys: Comparison with threshold events in mechanoreceptive afferent nerve fibers innervating the monkey hand," J. Neurophysiol. **35**, 122–136.
Park, J. T., Silvus, H. S., Jr., and Cerwin, S. A. (**1985**). "Active-wall device for the generation of small traveling surface waves," Rev. Sci. Instrum. **56**, 732–739.
Phillips, J. R., and Johnson, K. O. (**1981**). "Tactile spatial resolution. II. Neural representation of bars, edges, and gratings in monkey primary afferents," J. Neurophysiol. **46**, 1192–1203.
Robson, J. G. (**1966**). "Spatial and temporal contrast-sensitivity functions of the visual system," J. Opt. Soc. Am. **56**, 1141–1142.
Ruch, T. C. (**1946**). "The nervous system: Sensory functions," in *Howell's Textbook of Physiology*, edited by J. F. Fulton (Saunders, Philadelphia, PA).
Sato, M. (**1961**). "Response of Pacinian corpuscles to sinusoidal vibration," J. Physiol. **159**, 391–409.
Setzepfand, W. (**1935**). "Zur Frequenzabhangigkeit der Vibrationsempfindung des Menschen," Z. Biol. **96**, 236–240.
Shapley, R., and Lennie, L. (**1985**). "Spatial frequency analysis in the visual system," Ann. Rev. Neurosci. **8**, 547–583.
Sherrick, C. E. (**1953**). "Variables affecting sensitivity of the human skin to mechanical vibration," J. Exp. Psychol. **45**, 273–282.
Stevens, S. S., and Harris, J. R. (**1962**). "The scaling of roughness and smoothness," J. Exp. Psychol. **64**, 489–494.
Talbot, W. H., Darian-Smith, I., Kornhuber, H. H., and Mountcastle, V. B. (**1968**). "The sense of flutter-vibration: Comparison of the human capacity with response patterns of mechanoreceptive afferents from the monkey hand," J. Neurophysiol. **31**, 301–334.
Taylor, M. M. (**1971**). "On the efficiency of psychophysical measurement," J. Acoust. Soc. Am. **49**, 505–506.
Verrillo, R. T. (**1962**). "Investigation of some parameters of the cutaneous threshold for vibration," J. Acoust. Soc. Am. **34**, 1768–1773.
Verrillo, R. T. (**1963**). "Effect of contactor area on the vibrotactile threshold," J. Acoust. Soc. Am. **35**, 1962–1966.
Verrillo, R. T. (**1965**). "Temporal summation in vibrotactile sensitivity," J. Acoust. Soc. Am. **37**, 843–846.
Verrillo, R. T. (**1966**). "Specificity of a cutaneous receptor," Percept. Psychophys. **1**, 149–153.
Verrillo, R. T. (**1968**). "A duplex mechanism of mechanoreception," in *The Skin Senses*, edited by D. R. Kenshalo (Thomas, Springfield, IL).
Verrillo, R. T. (**1979**). "The effect of surface gradients on vibrotactile thresholds," Sens. Process. **3**, 27–36.
Vierck, C. J., Jr. (**1979**). "Comparisons of punctate, edge and surface stimulation of peripheral, slowly-adapting, cutaneous, afferent units of cat," Brain Res. **175**, 155–159.
Watson, A. B., and Pelli, D. G. (**1983**). "*QUEST*: A Bayesian adaptive psychometric method," Percept. Psychophys. **33**, 113–120.
Weinstein, S. (**1968**). "Intensive and extensive aspects of tactile sensitivity as a function of body part, sex, and laterality," in *The Skin Senses*, edited by D. R. Kenshalo (Thomas, Springfield, IL).
Zwislocki, J. J., Maire, F., Feldman, A. S., and Rubin, H. (**1958**). "On the effect of practice and motivation on the threshold of audibility," J. Acoust. Soc. Am. **30**, 254–262.